

Hadron Resonance Gas Model with Induced Surface Tension

V. V. Sagun^{1,2}, K. A. Bugaev^{1*}, A. I. Ivanytskyi¹, I. P. Yakimenko³, E. G. Nikonov⁴, A.V. Taranenko⁵, C. Greiner⁶, D. B. Blaschke^{5,7,8}, and G. M. Zinovjev¹

¹*Bogolyubov Institute for Theoretical Physics, Metrologichna str. 14^B, Kiev 03680, Ukraine*

²*CENTRA, Instituto Superior Técnico, Universidade de Lisboa, Av. Rovisco Pais 1, 1049-001 Lisboa, Portugal*

³*Department of Physics, Chemistry and Biology (IFM), Linköping University, SE-58183 Linköping, Sweden*

⁴*Laboratory for Information Technologies, JINR, Joliot-Curie str. 6, 141980 Dubna, Russia*

⁵*National Research Nuclear University “MEPhI” (Moscow Engineering Physics Institute), Kashirskoe Shosse 31, 115409 Moscow, Russia*

⁶*Institute for Theoretical Physics, Goethe University, Max-von-Laue-Str. 1, 60438 Frankfurt am Main, Germany*

⁷*Institute of Theoretical Physics, University of Wrocław, pl. M. Borna 9, 50-204 Wrocław, Poland*

⁸*Bogoliubov Laboratory of Theoretical Physics, JINR Dubna, Joliot-Curie str. 6, 141980 Dubna, Russia*
* E-mail: Bugaev@th.physik.uni-frankfurt.de

Abstract

Here we present a physically transparent generalization of the multicomponent Van der Waals equation of state in the grand canonical ensemble. For the one-component case the third and fourth virial coefficients are calculated analytically. It is shown that an adjustment of a single model parameter allows us to reproduce the third and fourth virial coefficients of the gas of hard spheres with small deviations from their exact values. A thorough comparison of the compressibility factor and speed of sound of the developed model with the one and two component Carnahan-Starling equation of state is made. It is shown that the model with the induced surface tension is able to reproduce the results of the Carnahan-Starling equation of state up to the packing fractions 0.2-0.22 at which the usual Van der Waals equation of state is inapplicable. At higher packing fractions the developed equation of state is softer than the gas of hard spheres and, hence, it breaks causality in the domain where the hadronic description is expected to be inapplicable. Using this equation of state we develop an entirely new hadron resonance gas model and apply it to a description of the hadron yield ratios measured at AGS, SPS, RHIC and ALICE energies of nuclear collisions. The achieved quality of the fit per degree of freedom is about 1.08. We confirm that the strangeness enhancement factor has a peak at low AGS energies, while at and above the highest SPS energy of collisions the chemical equilibrium of strangeness is observed. We argue that the chemical equilibrium of strangeness, i.e. $\gamma_s \simeq 1$, observed above the center of mass collision energy 4.3 GeV may be related to the hadronization of quark gluon bags which have the Hagedorn mass spectrum, and, hence, it may be a new signal for the onset of deconfinement.

1 Introduction.

Investigation of the strongly interacting matter equation of state (EoS) is the focus of modern nuclear physics and astrophysics [1, 2]. In the low density limit, the system can be considered as a statistical ensemble of composite particles which are characterized by their mass spectrum and their finite size. At higher densities, due to the requirement of antisymmetrisation of the wave function of the fermionic constituents, the Pauli blocking effect occurs which can be effectively modeled by the adoption of an excluded volume. At still higher densities the composites become unbound

and undergo a dissociation into their constituents (Mott effect). This effect was described first as an explanation of the insulator-to-metal transition [3] which occurs in some metal oxides under pressure. It has then been taken over to statistical plasma physics and the physics of liquids. In these systems, the finite size effects in the equation of state for composites are taken into account by a virial expansion which can be subsumed in a very compact form by the excluded volume concept leading, e.g., to the phenomenologically successful Carnahan-Starling EoS [4], see also [5, 6]. The proper description of cluster abundances in nuclear matter requires the account for excluded volume effects in the nuclear statistical equilibrium (for instance in supernova EoS [7, 8]) which on the more fundamental level are grounded in the Pauli principle leading to the Mott effect for clusters [9]. Most recently, the excluded volume concept has proven essential for the discussion of the deconfinement transition in compact stars, where a stiffening of the nuclear matter EoS due to the finite size of nucleons is a prerequisite for obtaining a novel type of hybrid star EoS allowing for so-called high-mass twin stars, a striking effect of quark deconfinement [10], potentially observable by precise mass and radius measurements on pulsars.

The hadron resonance gas model (HRGM) is not only a low energy density part of such an EoS, but it is also an important tool of heavy ion collisions phenomenology which allows one to obtain the parameters of chemical freeze-out (CFO) from experimental data [11, 12]. For more than two decades the HRGM was based on the Van der Waals EoS with one or two hard-core radii (one radius for mesons and another for baryons). Although recently there appeared new variations on the theme of excluded volume models [13] which allow a rather flexible modeling, in particular, of the nuclear EoS at supranuclear densities, the main phenomenological results were obtained by the HRGM with several hard-core radii [14, 15, 16, 17, 18, 19, 20, 21]. Indeed, such a model not only provides the high quality description of the hadron multiplicities from the lowest AGS collision energy of a few GeV to the LHC ALICE data measured at the center of mass collision energy $\sqrt{s_{NN}} = 2.76$ TeV, but it also allows one to study the subtlest features of hadron matter thermodynamics at CFO with very high confidence [14, 15, 16, 17, 18, 19, 20, 21]. Moreover, it allows one to find the novel irregularities and to suggest the new signals of the mixed phase formation in the nuclear collisions [18, 19, 22].

Alas, the presently existing N -component HRGM requires to solve N transcendental equations which may include contributions of hundreds of corresponding hadronic species. Therefore, further increasing the number of hard-core radii will lead to an essential increase in computational time which does not appear feasible. Moreover, in view of future experiments at the NICA-JINR and FAIR-GSI accelerators we expect to obtain many more experimental data with, hopefully, a higher accuracy. These new data will, in principle, allow us to study the second virial coefficients of the most abundant hadrons. Therefore, the development of a new multicomponent HRGM is necessary. The validity of this conclusion was demonstrated once more in [20] where a thorough analysis of the ALICE data within the conventional HRGM and with the bag-like prescription for hard-core radii suggested in [23] was performed.

Another restriction to use the HRGM appears due to the fact that the Van der Waals approximation accounts for the second virial coefficients only and, consequently, it can be safely applied to low densities, i.e. for packing fractions $\eta = \sum_{all\ hadrons} \rho_h V_h \leq 0.11$ [24] where V_h is the eigenvolume of hadron h and ρ_h is its particle number density. It is also necessary to note that the HRGM is the discrete part of the mass-volume spectrum of quark-gluon bag model with surface tension which has a tricritical [25] or a critical [26] endpoint. The quark-gluon bag model with surface tension model allows one to describe the properties of strongly interacting matter at high energy densities. In contrast to the HRGM the continuous part of the QGBSTM mass-volume spectrum, which describes the large and heavy quark-gluon-plasma bags employs the eigenvolume approximation. Note that this approximation is also used in all models describing the large and heavy quark-gluon-plasma

bags [25, 26, 27, 28, 29, 30, 31, 32, 33]. It is applicable at high energy densities or for $\eta > 0.3 - 0.4$, while at low packing fractions one has to employ the excluded volume model which reproduces the low density virial expansion. Therefore, the HRGM with the Van der Waals approximation, i.e. an excluded volume model (EVM), is traditionally used for many years. However, at the intermediate packing fractions $0.15 < \eta < 0.2$ the EVM may easily become inapplicable because of the superluminal values of the speed of sound [24, 20, 23]. Hence, an extension of the HRGM beyond the Van der Waals approximation is also necessary to model the strongly matter EoS near the region of transition between the hadron matter and quark gluon plasma.

Therefore, in this work we present a completely new version of the HRGM with the multicomponent hard-core repulsion which, by construction, is the Van der Waals EoS with the induced surface tension (IST EoS hereafter). This EoS is based on the virial expansion for multicomponent mixture and, hence, it naturally switches between the low and high density limits. Comparing it with the Carnahan-Starling EoS [4] for one and two particle species we find almost a perfect coincidence between them up to the packing fractions $\eta \simeq 0.2-0.22$. Its great advantage is that independently of the number of different hard-core radii the IST EoS is a system of only two transcendental equations. Using the IST EoS we successfully fit the traditional set of the hadron multiplicity ratios [14, 16, 17] measured at AGS, SPS, RHIC and ALICE energies of collisions.

The work is organized as follows. In Section 2 we present the IST EoS, calculate the third and fourth virial coefficients for the one-component case and compare this EoS with the Carnahan-Starling EoS. In Section 3 the necessary formalism is given and the results of fitting the hadron yields ratios are discussed. Our conclusions are summarized in Section 4. A heuristic derivation of the IST EoS is given in Appendix.

2 HRGM with the induced surface tension

A high quality description of the hadron yield ratios achieved in the last couple of years by the HRGM with multicomponent hard-core repulsion is a clear evidence of its great advantage over the one- and two- component versions. However, the main disadvantage of such a model is its mathematical complexity, which leads to an essentially longer time of numerical simulations. The HRGM [17] is a system of N transcendental equations, where N is the number of employed hard-core radii. Since in the HRGM all mesons, except for pions $R_\pi=0.1$ fm and kaons $R_K=0.395$ fm, have single hard-core radius $R_m \simeq 0.4$ fm and all baryons, except for Λ -hyperons $R_\Lambda=0.11$ fm, have their own value of hard-core radius $R_b=0.355$ fm, then the mesonic and baryonic equations include hundreds of terms corresponding to accounted hadron states. Although these hard-core radii provide very high quality description of 111 independent particle yield ratios measured in the central nuclear collisions for the center of mass collision energies $\sqrt{s_{NN}} = 2.7, 3.3, 3.8, 4.3, 4.9, 6.3, 7.6, 8.8, 9.2, 12, 17, 62.4, 130$ and 200 GeV (for the details see [14, 16, 17]) with $\chi^2/dof \simeq 0.95$ [17], any further increase of the number of independent hadronic hard-core radii in the HRGM will face severe computational difficulties. More details on the HRGM equations and the list of experimental data employed in the actual simulations can be found in [14, 15, 16, 17].

Here we employ a more effective model with multicomponent hard-core repulsion named the IST EoS because besides the hard-core repulsion it explicitly contains the surface tension induced by the inter particle interaction [34]. Recently, such an EoS was proposed on the basis of the virial expansion of multicomponent mixture [34] obtained for the simplified statistical multifragmentation model [35] with an infinite number of hard-core radii of nuclear fragments of all sizes. Such an EoS is a system of coupled equations between the system pressure p and the induced surface tension coefficient Σ which has the form [20, 34] (for convenience, its simplified derivation is given in

Appendix)

$$p = T \sum_{k=1}^N \phi_k \exp \left[\frac{\mu_k}{T} - \frac{4}{3} \pi R_k^3 \frac{p}{T} - 4\pi R_k^2 \frac{\Sigma}{T} \right], \quad (1)$$

$$\Sigma = T \sum_{k=1}^N R_k \phi_k \exp \left[\frac{\mu_k}{T} - \frac{4}{3} \pi R_k^3 \frac{p}{T} - 4\pi R_k^2 \alpha \frac{\Sigma}{T} \right], \quad (2)$$

$$\mu_k = \mu_B B_k + \mu_{I3} I_{3k} + \mu_S S_k. \quad (3)$$

Here μ_B , μ_S , μ_{I3} are, respectively, the baryonic, the strange and the third projection of isospin chemical potentials, while B_k , S_k , I_{3k} , m_k and R_k denote, respectively, the corresponding charges, mass and hard-core radius of the k -sort of hadrons. The summations in Eqs. (1) and (2) are made over all sorts of hadrons and their antiparticles are considered as independent species.

In Eq. (2) the dimensionless parameter $\alpha > 1$ is introduced due to the freedom of the Van der Waals extrapolation to high densities [34]. As it is shown below, the parameter α accounts for the high density terms of virial expansion and it allows us to modify the Van der Waals EoS to a more realistic one. In principle, α can be a regular function of T and μ , however, for the sake of simplicity it is fixed to a constant value.

The one-particle thermal density ϕ_k in Eqs. (1) and (2) accounts for the Breit-Wigner mass attenuation and is written in the Boltzmann approximation

$$\phi_k = g_k \gamma_S^{|s_k|} \int_{M_k^{Th}}^{\infty} \frac{dm}{N_k(M_k^{Th})} \frac{\Gamma_k}{(m - m_k)^2 + \Gamma_k^2/4} \int \frac{d^3p}{(2\pi)^3} \exp \left[-\frac{\sqrt{p^2 + m^2}}{T} \right], \quad (4)$$

for all hadrons except pions. Here g_k is the degeneracy factor of the k -sort of hadrons, γ_S is the strangeness suppression factor [40], $|s_k|$ is the number of valence strange quarks and antiquarks in this kind of hadrons, $N_k(M_k^{Th}) \equiv \int_{M_k^{Th}}^{\infty} \frac{dm \Gamma_k}{(m - m_k)^2 + \Gamma_k^2/4}$ denotes a corresponding normalization, while

M_k^{Th} corresponds to the decay threshold mass of the k -sort of hadrons. We would like to point out the fact that usage of the mass attenuation like in Eq. (4) for a mixture of hadron resonances can be rigorously derived [36, 37] from the Phi-functional approach [38], when the Phi-functional is chosen from the class of two-loop diagrams only, see also [39].

For the pions of sort $A = \{-, 0, +\}$, instead of the Boltzmann distribution (4) we use the Bose-Einstein distribution function

$$\phi_{\pi_A} = \int \frac{d^3p}{(2\pi)^3} \frac{1}{\exp \left[\frac{\sqrt{p^2 + m_\pi^2} - \mu_{I3} I_{3,A}}{T} \right] - 1}, \quad (5)$$

because at high temperatures, which will be analyzed here, the quantum correction cannot be ignored. Here the particle density of pions depends on the third projection of isospin $I_{3,A}$ and the corresponding chemical potential μ_{I3} .

The system of Eqs. (1), (2) and (3) should be supplemented by the strange charge conservation law, which in case of relativistic collisions of heavy ions has the form

$$\sum_{k=1}^N \phi_k S_k \exp \left[\frac{\mu_k}{T} - \frac{4}{3} \pi R_k^3 \frac{p}{T} - 4\pi R_k^2 \frac{\Sigma}{T} \right] = 0, \quad (6)$$

which completes the system of equations employed for analysis of hadron multiplicities.

In the work [34] it was established that the parameter α should be greater than one in order to reproduce the physically correct phase diagram properties of nuclear matter. In order to determine the correct value of parameter α , we compare here the IST EoS for the point-like pions, for the nucleons and $\Delta(1232)$ baryons having the same hard-core radius of 0.4 fm with the famous Carnahan-Starling EoS [4] found for the same temperature, same particle densities and same hard-core radii. For simplicity the antibaryons are neglected in this treatment.

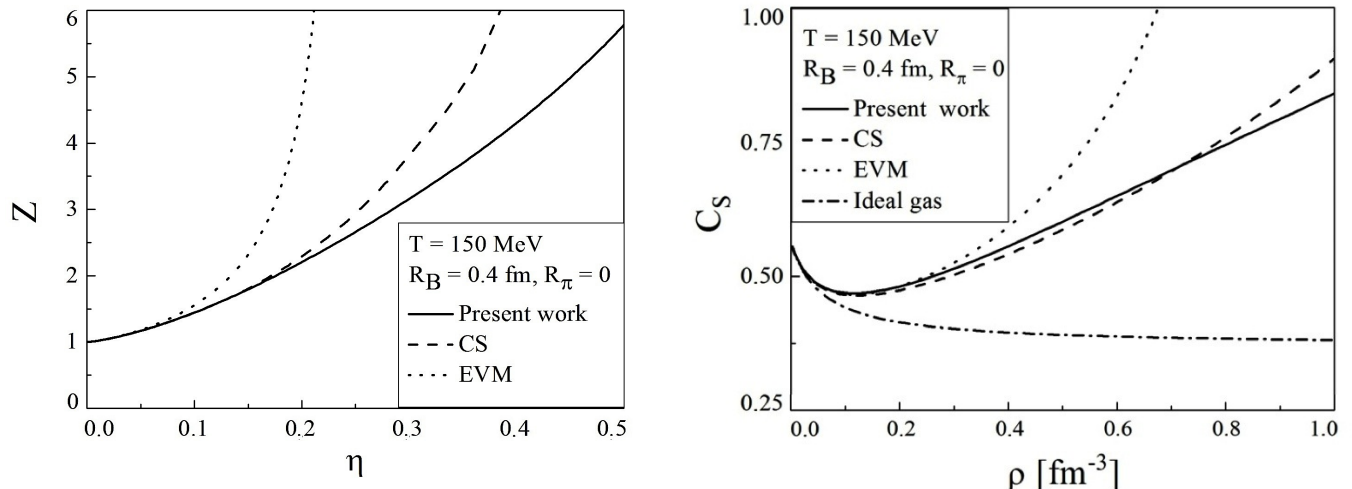


Figure 1: **Left panel:** Compressibility factor Z of the gas consisting from the point-like pions, the nucleons and $\Delta(1232)$ baryons having the hard-core radius of 0.4 fm is shown for different EoS as a function of baryon packing fraction η . The Van der Waals EoS (dotted curve), the IST EoS (solid curve) and CS EoS (long dashed curve) are shown for $T = 150$ MeV. **Right panel:** The speed of sound as a function of baryonic density is shown for the same EoS as in the left panel and with the same notations. The dotted-dashed curve shows the speed of sound for point-like pions and baryons.

In order to further simplify a comparison we consider the case $\mu_{I3} = \mu_S = 0$, while $\mu_B > 0$. Then the Carnahan-Starling EoS [4] for the mixture of baryons (the nucleons and $\Delta(1232)$ baryons) and point-like pions is [24]

$$P^{CS} = 3T\phi_{\pi_0}(T) + \rho_B T Z_B, \quad Z_B = \frac{1 + \eta + \eta^2 - \eta^3}{(1 - \eta)^3}, \quad (7)$$

where the packing fraction of baryons of the same hard-core radius R is $\eta = \frac{4}{3}\pi R^3 \rho_B$ and ρ_B is their baryon density $\rho_B \equiv \frac{\partial p}{\partial \mu_B}$ and pion number density $\rho_\pi \equiv \frac{\partial p}{\partial \mu_\pi} \Big|_{\mu_\pi=0}$ can be found from Eq. (7) and from the system (1)-(5) for a comparison. More details on calculating the particle densities and speed of sound for Eq. (7) can be found in [24] (see Eqs. (59)-(64)), while the necessary expressions for the particle densities of the IST EoS are given below (see Eqs. (21) and (26)). As one can see from Figs. 1 and 2 the IST EoS with $\alpha = 1.25$ reproduces the compressibility factor $Z \equiv \frac{p}{T(\rho_B + 3\rho_{\pi_0}(T))}$ up to $\eta \simeq 0.22$. From these figures one can also see that the speed of sound c_s of (7) is almost perfectly reproduced by the IST EoS with $\alpha = 1.25$ up to five values of normal nuclear density ($\eta \simeq 0.22$). These figures also show that the EVM can be used up to $\eta \simeq 0.11$ [24].

Note that such a comparison is justified by the fact that the hard-core radii found by the HRGM in [17] are close to 0.4 fm, except for pions and Λ -hyperons which are about 0.1 fm, i.e.

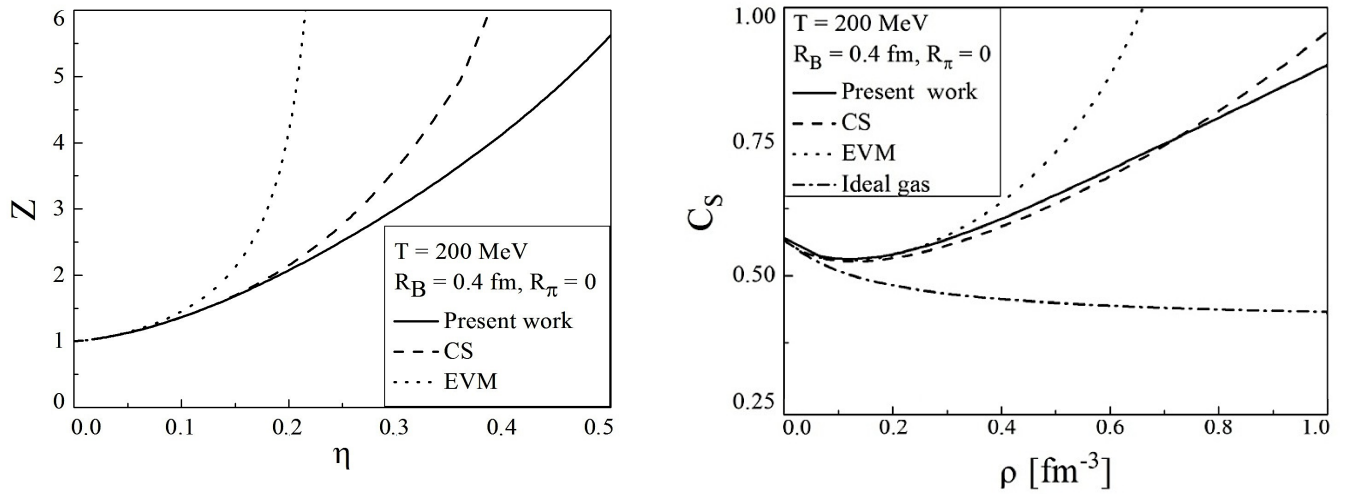


Figure 2: Same as in Fig. 1, but for $T = 200$ MeV.

their eigenvolume is about $4^3 = 64$ times smaller than the one of other hadrons. Although these hard-core radii were found within the range of applicability of the EVM approximation, we expect that fitting the same data with the IST EoS (1)-(5) will not drastically change their values.

In order to reveal the reason for such a good correspondence between the Carnahan-Starling EoS and the IST EoS with $\alpha = 1.25$ we calculate the third and fourth virial coefficients of the system (1)-(5) for the same hard-core radius R and for the same (baryonic) charge of particles, i.e. for $\{R_k\} = R$ and $\{B_k\} = 1$ for any k . Then differentiating Eqs. (1) and (2) with respect to $\mu_k = \mu$ and excluding from them the derivative

$$\frac{\partial \Sigma}{\partial \mu} = \frac{\Sigma (1 - v\rho)}{T \left(1 + \frac{\alpha s \Sigma}{T}\right)}, \quad (8)$$

one can find the following expression for particle density

$$\rho \equiv \frac{\partial p}{\partial \mu} = \frac{p}{T} (1 - v\rho) \frac{1 + \frac{(\alpha-1)s\Sigma}{T}}{1 + \frac{\alpha s \Sigma}{T}}. \quad (9)$$

Here $v = \frac{4}{3}\pi R^3$ and $s = 4\pi R^2$ are, respectively, the eigenvolume and eigensurface of particles of hard-core radius R . Dividing Eq. (2) for $\{R_k = R\}$ by Eq. (1) for $\{R_k = R\}$, one can establish a useful identity

$$\Sigma = p R \exp \left[-s \cdot (\alpha - 1) \frac{\Sigma}{T} \right] \equiv p R E_{\Sigma}. \quad (10)$$

Using the identity (10), one can identically rewrite (9) in the form

$$p = \frac{T \rho}{\left[1 - v\rho - \frac{3v\rho E_{\Sigma}}{1 + \frac{(\alpha-1)3v\rho E_{\Sigma}}{T}} \right]} \quad (11)$$

$$\equiv \frac{T \rho}{[1 - v^{eff}\rho]}. \quad (12)$$

Expression (11) is convenient for further evaluation. Here we used an evident relation $sR = 3v$. From the denominator of (11) one can find an effective excluded volume of particle

$$v^{eff} = v \left[1 + \frac{3E_\Sigma}{1 + \frac{(\alpha-1)3vpE_\Sigma}{T}} \right]. \quad (13)$$

This expression shows that at low densities, i.e. for $\frac{|\alpha-1|s\Sigma}{T} \ll 1$, and from (10) one obtains $E_\Sigma \rightarrow 1$; and hence $v^{eff} \simeq 4v$ correctly reproduces the excluded volume. In the high density limit, on the other hand, $\frac{pv}{T} \gg 1$ and, hence, $\frac{(\alpha-1)s\Sigma}{T} \gg 1$ since $\mu/T \rightarrow \infty$. Therefore, for $\alpha > 1$ one finds that $E_\Sigma \rightarrow 0$ and the effective excluded volume in Eq. (12) becomes equal to the eigenvolume, i.e. $v^{eff} \simeq v$. Thus, in the IST EoS the parameter α switches between the excluded volume and the eigenvolume regimes. Also from Eqs. (10) and (12) one can find that for $\alpha = 1$ it follows that $v^{eff} = 4v$, i.e. the IST EoS recovers the usual EVM result.

Expanding the denominator in (11) in a geometric series, expanding E_Σ in the Taylor series in powers of Σ , and applying the aforementioned identity (10) to them one can get the following result for the pressure of the one-component Boltzmann gas

$$p \simeq T\rho(1 + 4v\rho + B_3\rho^2 + B_4\rho^3 + \dots), \quad (14)$$

$$B_3 = [16 - 18(\alpha - 1)]v^2, \quad (15)$$

$$B_4 = \left[64 + \frac{243}{2}(\alpha - 1)^2 - 216(\alpha - 1) \right]v^3, \quad (16)$$

where in the intermediate steps we substituted the virial expansion (14) into the right hand side of (11). Comparing this result with the virial expansion of the one-component gas of hard spheres [41]

$$p \simeq T\rho(1 + 4v\rho + 10v^2\rho^2 + 18.36v^3\rho^3 + \dots), \quad (17)$$

one finds that $B_3(\alpha = 4/3) = 10v^2$, but, unfortunately, in this case $B_4(\alpha = 4/3) \simeq 5.5v^3$, which is too small compared to $18.36v^3$. On the other hand, solving an equation

$$B_4(\alpha) = 18.36v^3, \quad (18)$$

one finds two solutions $\alpha_1 \simeq 1.245$ and $\alpha_2 \simeq 2.533$. Since $B_3(\alpha = \alpha_1) \simeq 11.59v^2$ and $B_3(\alpha = \alpha_2) \simeq -11.59v^2$, it is evident that the correct root is $\alpha = \alpha_1 \simeq 1.245$. This is an indication of a very good correspondence between the Carnahan-Starling EoS (7) and the IST EoS with $\alpha = 1.25$; in fact, $B_3(\alpha = 1.25) \simeq 11.5v^2$ and $B_4(\alpha = 1.25) \simeq 17.59v^3$. In other words, the one-component IST EoS reproduces the third virial coefficient of the gas of hard spheres with the relative error +15% and the fourth virial coefficient with the relative error -4.1%. Note that at the packing fraction $\eta = v\rho = 0.2$ the deviation of the compressibility factor $Z(\eta) = \frac{p}{T\rho}$ generated by these errors is, respectively, $1.5\eta^2 \simeq 0.06$ and $-0.766\eta^3 \simeq -0.006$, which should be compared to the value $Z(0.2) \simeq 2$. In other words, at the packing fraction $\eta = 0.2$ the relative deviation of the IST EoS $Z(0.2)$ from the one of hard spheres is less than 3%! Clearly, for $\eta < 0.2$ the deviation of the IST EoS from the EoS of hard spheres and from the Carnahan-Starling EoS is much smaller.

To illustrate the validity of this conclusion in the left panel of Fig. 3 we compare the Carnahan-Starling EoS and the IST EoS with $\alpha = 1.25$ for the nucleons, $\Delta(1232)$ baryons and pions of the same hard-core radius $R = 0.4$ fm. As one can see from this figure the coincidence of these two EoS is the same as for the Carnahan-Starling EoS with point-like pions demonstrated in Figs. 1 and 2. Thus, here we showed that the IST EoS with a single additional parameter α compared to the EVM is not only able to reproduce the second virial coefficient, but it is also able to reproduce the

third and fourth virial coefficients of the gas of hard spheres very well! Therefore, in this work we employ the value $\alpha = 1.25$.

From the right panel of Fig. 3 one can see that the one-component IST EoS gets softer and the region of its causality widens, if the common hard-core radius of hadrons decreases.

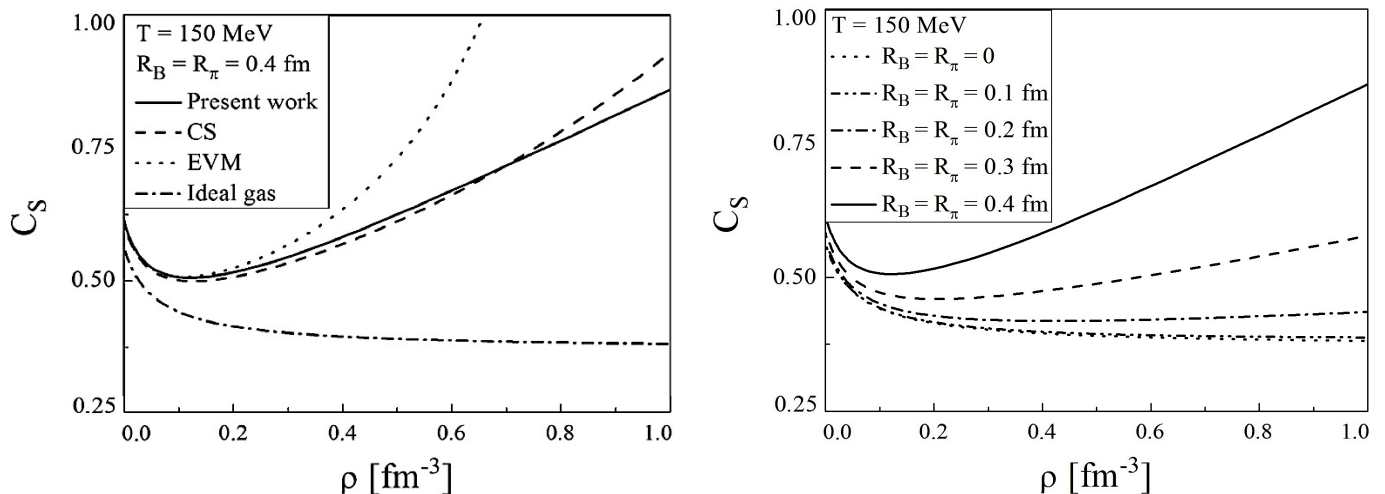


Figure 3: **Left panel:** The speed of sound of the gas consisting from the pions, the nucleons and $\Delta(1232)$ baryons having the same hard-core radius of 0.4 fm is shown for different EoS. The Van der Waals EoS (dotted curve), the IST EoS (solid curve) and CS EoS (long dashed curve) are shown for $T = 150$ MeV. **Right panel:** The speed of sound of one-component IST EoS as a function of baryonic density is shown for the same gas as in the left panel, but for different values of hard-core radius.

3 Fitting the hadron yield ratios

The fit procedure along with the detailed description of the experimental set of 111 independent ratios used here is very well documented in [14, 17, 21] and, hence, there is no reason to repeat this well known information. The data are the ratios measured in the central nuclear collisions for the center of mass collision energies $\sqrt{s_{NN}} = 2.7, 3.3, 3.8, 4.3, 4.9$ (AGS energies), 6.3, 7.6, 8.8, 12, 17 (NA49 data), 9.2, 62.4, 130 and 200 GeV (STAR data). Here we do not analyze the Beam Energy Scan data measured at RHIC, since these data are rather preliminary and, consequently, they often have rather large error bars even for the hadronic multiplicities, hence, we do not think that a fit of these data will give us any new information about the thermodynamics of CFO. Nevertheless, in addition to the data measured at AGS, SPS and RHIC energies, we analyze the ALICE data [42, 43, 44, 45, 46, 47, 48] from which the independent ratios were prepared in [20].

A few remarks should be made here about the ALICE data used in a fit. Similarly to Ref. [12] we do not include the K^* data into the fitting procedure, since the reactions like $K + \pi \leftrightarrow K^*$ can occur after chemical freeze-out and change the K^* yields [12]. For a detailed explanation see the caption of Fig. 1 in [12]. However, in contrast to [12] we do not include into a fit the ratios which involve the (anti)nuclei. Although, similarly to [12], it is possible to fit the full set of the ALICE data [42, 43, 44, 45, 46, 47, 48] with the HRGM [20], we do not think that taking the hard-core radius of (anti)nuclei to be the same as for baryons is a correct approach.

Ratio	Value	Error
π^-/π^+	0.99776	0.10023
K^-/K^+	0.99500	0.11645
\bar{p}/p	0.98387	0.11313
Ξ^-/Ξ^+	1.01829	0.10552
Ω^-/Ω^+	0.96667	0.23371
ϕ/K^-	0.11250	0.02500
p/π^+	0.04630	0.00500
K^+/π^+	0.14937	0.01605
Λ/π^+	0.03585	0.00453
Ξ^+/π^+	0.00490	0.00050
Ω^+/π^+	0.00090	0.00016

Table 1: Ratios which were obtained in [20] and which are analyzed here.

3.1 Necessary Formalism

To fit the ratios we need the explicit expressions for the particle number densities. Introducing the partial pressure p_k and the partial surface tension coefficient Σ_k of a hadron of sort k

$$p_k = T\phi_k \exp\left[\frac{\mu_k}{T} - \frac{4}{3}\pi R_k^3 \frac{p}{T} - 4\pi R_k^2 \frac{\Sigma}{T}\right], \quad (19)$$

$$\Sigma_k = T R_k \phi_k \exp\left[\frac{\mu_k}{T} - \frac{4}{3}\pi R_k^3 \frac{p}{T} - 4\pi R_k^2 \alpha \frac{\Sigma}{T}\right] \equiv p_k R_k \exp\left[-4\pi R_k^2 (\alpha - 1) \frac{\Sigma}{T}\right], \quad (20)$$

one can get the particle number density of hadrons of sort k as

$$\rho_k \equiv \frac{\partial p}{\partial \mu_k} = \frac{1}{T} \cdot \frac{p_k a_{22} - \Sigma_k a_{12}}{a_{11} a_{22} - a_{12} a_{21}}, \quad (21)$$

where the coefficients a_{kl} can be expressed in terms of the partial pressures $\{p_k\}$ and the partial surface tension coefficients $\{\Sigma_k\}$ as

$$a_{11} = 1 + \frac{4}{3}\pi \sum_k R_k^3 \frac{p_k}{T}, \quad (22)$$

$$a_{12} = 4\pi \sum_k R_k^2 \frac{p_k}{T}, \quad (23)$$

$$a_{21} = \frac{4}{3}\pi \sum_k R_k^3 \frac{\Sigma_k}{T}, \quad (24)$$

$$a_{22} = 1 + 4\pi\alpha \sum_k R_k^2 \frac{\Sigma_k}{T}. \quad (25)$$

In case of the pion-like particles, say pions ($R_\pi = 0$), the expression (21) is simplified as

$$\rho_\pi \equiv \left. \frac{\partial p}{\partial \mu_\pi} \right|_{\mu_\pi=0} = \frac{1}{T} \cdot \frac{p_\pi}{a_{11} - \frac{a_{12} a_{21}}{a_{22}}}, \quad (26)$$

$$\rho_\pi \xrightarrow[\text{low densities}]{} \frac{1}{T} \cdot \frac{p_\pi}{1 + \frac{4}{3}\pi \sum_k R_k^3 \frac{p_k}{T}}, \quad (27)$$

which can be simplified further at low densities, as it is seen from Eq. (27), since in this limit one can safely neglect in (26) the product $a_{12} a_{21}$ compared to a_{22} . This expression demonstrates the meaning of the hard-core interaction for point-like particles. Indeed, at low densities the partial pressure of each hadron is close to the ideal gas one, i.e. $p_k \simeq T\rho_k$, and, hence, a sum in the denominator of Eq. (27) accounts for the fact that the point-like pions cannot occupy the volume which is already filled up by the eigenvolumes of all other particles. We note that Eqs. (21) and (26) were used, respectively, to evaluate the density of baryons and point-like pions for a comparison between the IST EoS and the EoS given by (7).

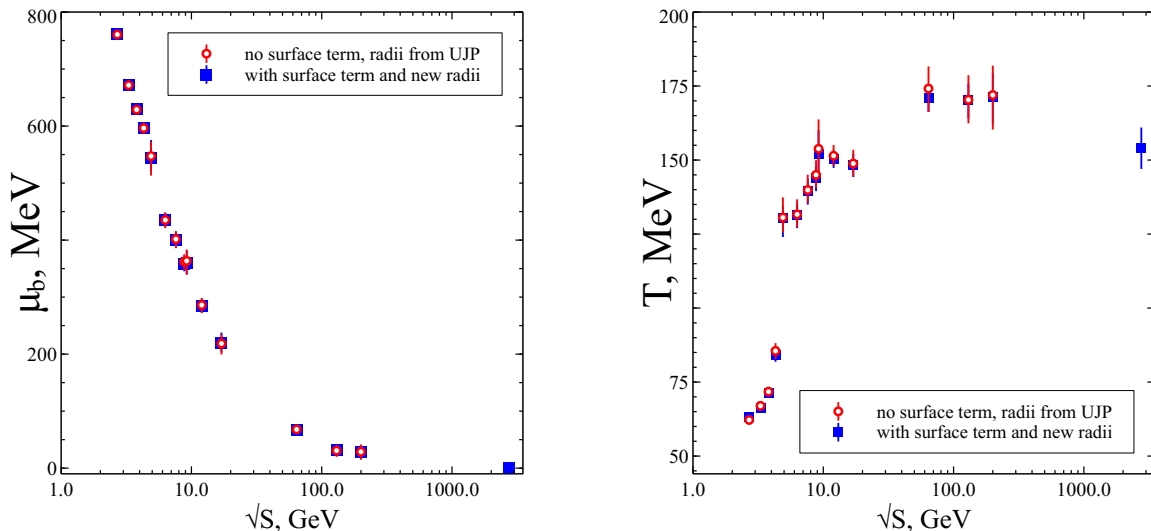


Figure 4: Chemical freeze-out parameters of the IST EoS (circles) are compared to the ones found within the HRGM with multicomponent hard-core repulsion (squares) [17]. Left and right panels show, respectively, the center of mass collision energy dependence of the baryonic chemical potential and temperature.

The contribution of the resonance decays is taken into account as usual: the total density of hadron X consists of the thermal part n_X^{th} and the decay ones:

$$n_X^{tot} = n_X^{th} + n^{decay} = n_X^{th} + \sum_Y n_Y^{th} Br(Y \rightarrow X), \quad (28)$$

where $Br(Y \rightarrow X)$ denotes the decay branching of the Y -th hadron into the hadron X . The masses, the widths and the strong decay branchings of all hadrons were taken from the particle tables used by the thermodynamic code THERMUS [49].

3.2 Results for AGS, SPS and RHIC energies

The parameter $\alpha = 1.25$ is used to fit 111 independent hadron ratios measured at AGS, SPS and RHIC energies with the IST EoS. In this fit the factor γ_s and the chemical potentials μ_B and μ_{I3} are used as the free parameters and we found that the best description of these data is reached for the following hard-core radii of baryons $R_b=0.365$ fm, mesons $R_m=0.42$ fm, pions $R_\pi=0.15$ fm, kaons $R_K=0.395$ fm and Λ -hyperons $R_\Lambda=0.085$ fm. These values of the hard-core radii generate $\chi_1^2/dof = 57.099/55 \simeq 1.038$.

Compared to the values found by the HRGM [17], i.e. the hard-core radii of baryons $R_b=0.355$ fm, mesons $R_m=0.4$ fm, pions $R_\pi=0.1$ fm, kaons $R_K=0.395$ fm and Λ -hyperons $R_\Lambda=0.11$ fm, the hard-core radii of the IST EoS R_b , R_m and R_K are practically unchanged, while the pionic hard-core

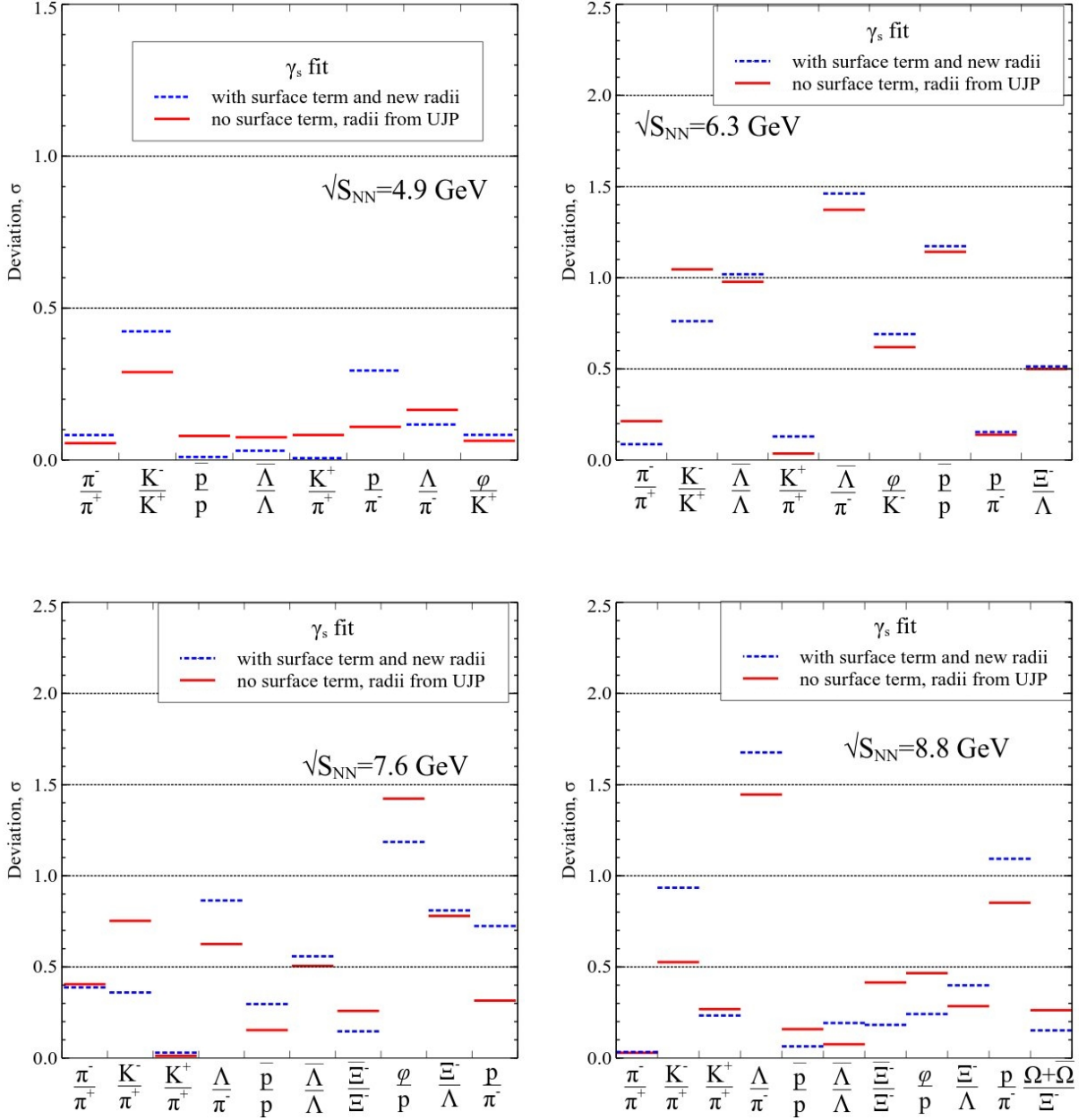


Figure 5: Deviations of theoretically predicted hadronic yield ratios from experimental values in units of experimental error σ are shown for the center of mass collision energies $\sqrt{s_{NN}} = 4.9, 6.3, 7.6, 8.8$ GeV. Dashed lines correspond to the IST EoS fit, while the solid lines correspond to the original HRGM fit [17].

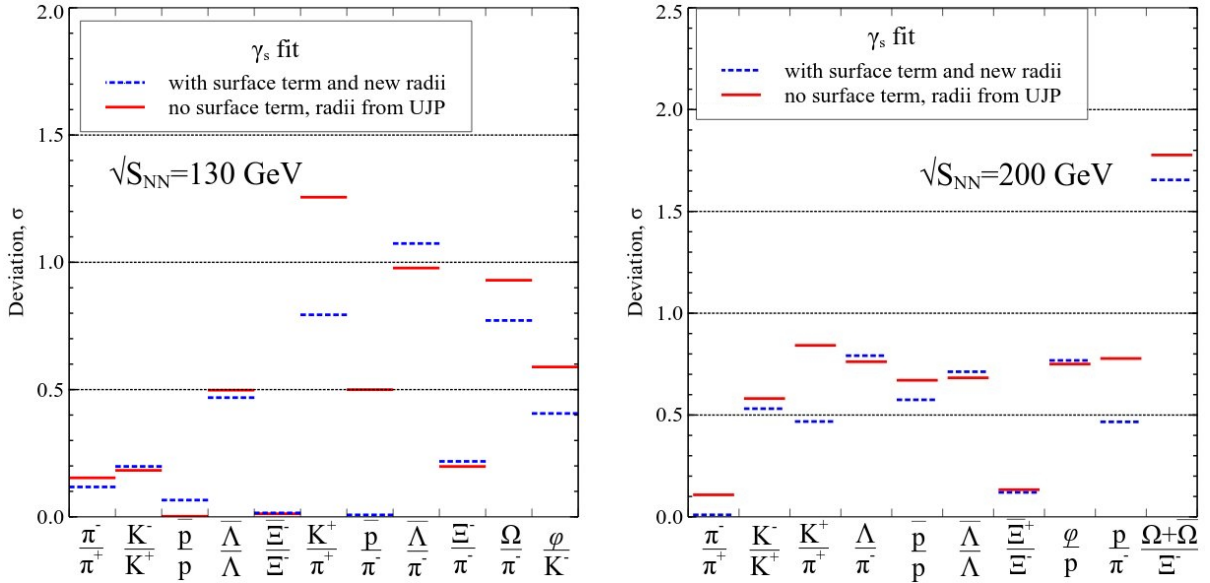


Figure 6: Same as in Fig. 5, but for the center of mass collision energies $\sqrt{s_{NN}} = 130$ GeV and $\sqrt{s_{NN}} = 200$ GeV.

radius is increased by 50% and the hard-core radius of Λ -hyperons is diminished by 20%. From Fig. 4 one can see that, despite the different hard-core radii of pions and Λ -hyperons, the collision energy dependence of the baryonic chemical potential and temperature at CFO are unchanged compared to the HRGM [17]. The sudden jump of the CFO temperature observed between the collision energies $\sqrt{s_{NN}} = 4.3$ GeV and $\sqrt{s_{NN}} = 4.9$ GeV also remains unchanged. This is an important finding since such an irregularity, analyzed for the first time in [18], led to a discovery of possible signals of the mixed phase formation in the central nuclear collisions [18, 19].

Some typical results of the IST EoS fit are compared with the ones of HRGM in Figs. 5 and 6. As one can see from these figures at the collision energies $\sqrt{s_{NN}} = 4.9$ GeV, $\sqrt{s_{NN}} = 6.3$ GeV and $\sqrt{s_{NN}} = 200$ GeV the quality of the IST EoS fit is almost the same as the one achieved with the HRGM. At the collision energies $\sqrt{s_{NN}} = 7.6$ GeV and $\sqrt{s_{NN}} = 130$ GeV one can find an improved description of the ϕ -meson to proton ratio and the K^+ -meson to π^+ -meson ratio, respectively, while at $\sqrt{s_{NN}} = 8.8$ GeV we found a slight worsening in the description of proton to π^- -meson ratio and in the ratio Λ/π^- (see Fig. 5). The fit results for other collision energies obtained by the HRGM and by the IST EoS are hardly distinguishable from each other.

We would like to mention that the IST EoS provides an improvement of the K^+/π^+ description (the Strangeness Horn) from $\chi^2/dof \simeq 3.92/14$ in [17] to $\chi^2/dof \simeq 3.29/14$ here, while $\sqrt{s_{NN}}$ dependences of Λ/π^- and $\bar{\Lambda}/\pi^-$ ratios are reproduced here with $\chi^2/dof \simeq 11.62/12$ and $\chi^2/dof \simeq 8.89/8$, respectively. Compared to the fit qualities $\chi^2/dof \simeq 10.22/12$ for Λ/π^- and $\chi^2/dof \simeq 6.49/8$ for $\bar{\Lambda}/\pi^-$ obtained in [17], the present results are slightly worse, but still they are rather good. The collision energy dependence of these ratios is shown in Fig. 7.

The other important finding is that the collision energy dependence of the factor γ_s for the IST EoS is practically the same as for the HRGM of Ref. [17]. Thus, the factor γ_s demonstrates a low sensitivity to the IST EoS, which means that the present model confirms an existence of a strangeness enhancement at low collision energies, namely the peak of the factor γ_s is found at $\sqrt{s_{NN}} = 3.8$ GeV as one can see from Fig. 7. Besides, this figure shows that for $\sqrt{s_{NN}} \geq 4.9$ GeV there is chemical equilibrium of strange charge, since $\gamma_s \simeq 1$ within the error bars. One possible explanation of such a behavior is an appearance of quark gluon bags with the Hagedorn (exponential) mass spectrum [50]. Since such a mass spectrum acts as a perfect thermostat and a perfect chemical reservoir [51]

one may expect that the hadrons appearing at the moment of quark gluon bag hadronization will be born in a full thermal and chemical equilibrium [51, 52, 53, 54]. We would like to stress that this conclusion is in line with the recent finding that the mixed quark-gluon-hadron phase is created at the collision energy range between $4.3 \text{ GeV} < \sqrt{s_{NN}} \leq 4.9 \text{ GeV}$ [18, 19, 22]. Hence, the observed change of the collision energy dependence regime of γ_s at $\sqrt{s_{NN}} \simeq 4.9 \text{ GeV}$ maybe another evidence for the onset of deconfinement.

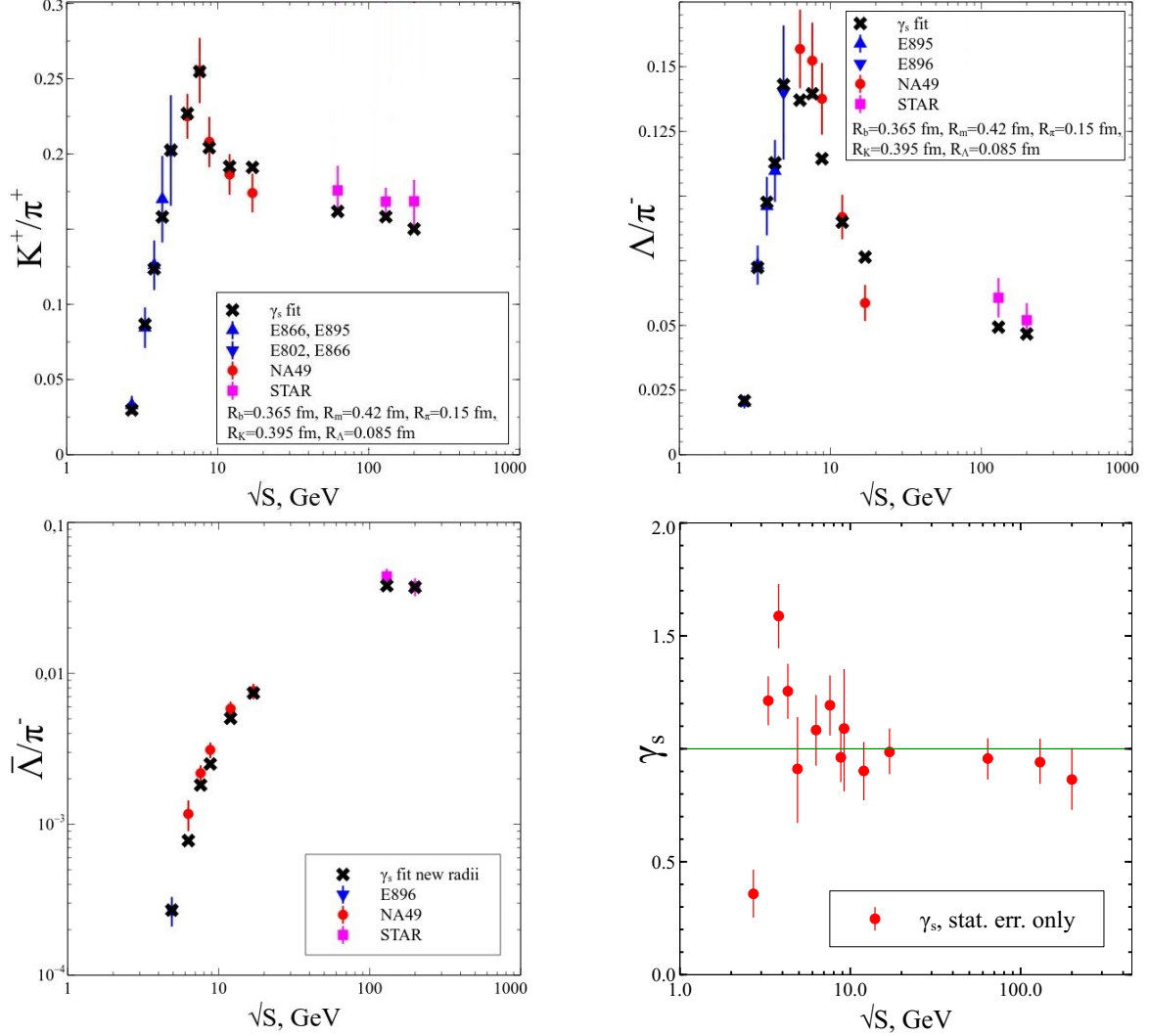


Figure 7: The fit results obtained by the IST EoS. **Upper left panel:** $\sqrt{s_{NN}}$ dependence of K^+/π^+ . **Upper right panel:** $\sqrt{s_{NN}}$ dependence of Λ/π^- . **Lower left panel:** $\sqrt{s_{NN}}$ dependence of $\bar{\Lambda}/\pi^-$. **Lower right panel:** $\sqrt{s_{NN}}$ dependence of the factor γ_s .

3.3 Results for ALICE energy

To fit the ALICE data [42, 43, 44, 45, 46, 47, 48] we use a different strategy. The reason is that the fit quality is not sensitive to the values of the hard-core radii. In fact, even the HRGM with the point-like particles provides a reasonable fit quality [20, 55]. Therefore, in order to avoid the unnecessary waste of CPU time we adopted the new radii found in this work from fitting the AGS, SPS and RHIC data, then, similarly to [12], we set all values of chemical potentials to zero, but the factor γ_s is fixed as $\gamma_s = 1$. Thus, for the ALICE data we come up with 11 independent ratios (see Table 1)

and with a single fitting parameter, namely the CFO temperature which is found $T_{CFO} \simeq 152 \pm 7$ MeV. Within the error bars this result is in agreement with the similar fits [12, 55]. The achieved description of the ALICE data is shown in Fig. 8. The fit quality $\chi^2/dof \simeq 8.04/5 \simeq 1.61$ of the ALICE data is slightly worse than the one found for the combined fit of the AGS, SPS and RHIC data. From Fig. 8 one can see that the main part of χ^2 is generated by only two ratios, i.e. p/π^+ and Λ/π^+ . Therefore, the combined quality of the AGS, SPS, RHIC and ALICE data description achieved in the present work is $\chi^2_{tot}/dof \simeq 65.1/60 \simeq 1.08$.

Although the found CFO temperature for the ALICE data is rather low, we note that a priori it was not clear what maximal value for T_{CFO} has to be chosen. For example, the authors of Ref. [23] claimed that they found the second minimum of χ^2/dof for the ALICE data which is located at the temperature about 274 MeV. Of course, it is hard to believe that at so high temperature the hadrons may exist and that at so huge particle densities the inelastic reactions are frozen, but in order not to miss the χ^2/dof minimum at high temperatures we performed its minimization for $T_{CFO} < 600$ MeV.

Although one can formally employ the IST EoS at any temperature, first we would like to determine the temperature range of its applicability. For this purpose we employ the multicomponent version of the Carnahan-Starling EoS known as the MCSL EoS [56]. Such an EoS is well known in the theory of simple liquids [57, 58]. Similarly to its one-component counterpart [4] the MCSL EoS rather accurately reproduces the pressure of hard spheres until the packing fraction values $\eta \leq 0.35 - 0.4$ [56, 58]. As usual, the packing fraction of the N -component mixture $\eta \equiv \sum_{k=1}^N \frac{4}{3} \pi R_k^3 \rho_k$ is defined via the set of hard-core radii $\{R_k\}$ and the corresponding particle densities $\{\rho_k\}$. In terms of these notations the MCSL pressure [56] can be cast as

$$p^{CS} = \frac{6T}{\pi} \left[\frac{\xi_0}{1 - \xi_3} + \frac{3\xi_1\xi_2}{(1 - \xi_3)^2} + \frac{3\xi_2^3}{(1 - \xi_3)^3} - \frac{\xi_3\xi_2^3}{(1 - \xi_3)^3} \right], \quad (29)$$

$$\xi_n = \frac{\pi}{6} \sum_{k=1}^N \rho_k [2R_k]^n. \quad (30)$$

Using the system (29), (30) we can find out the applicability bounds of the IST EoS at high temperatures by comparing the IST EoS pressure (1) with the MCSL pressure (29) which we calculate for the same set of particle densities $\{\rho_k\}$ given by Eq. (21). The results for the compressibility $Z = p/(\rho T)$ are given in Fig. 9. Here the total pressure of the system is p , while the total particle density is $\rho = \sum_{k=1}^N \rho_k$.

From the left panel of Fig. 9 one can see that for $T \leq 275$ MeV the IST EoS obeys the condition applicability $\eta < 0.22$. Note also that at $T \simeq 275$ MeV the IST EoS provides a 5% deviation from the MCSL EoS at $T \simeq 275$ MeV, i.e. in the region where the second minimum of χ^2/dof is observed in the work [23]. But in contrast to Ref. [23], we do not observe any additional minimum in our model up to $T = 600$ MeV. A detailed analysis of the ALICE data for different versions of the HRGM can be found in [20].

An entirely different situation is for the EVM. In contrast to the IST EoS, the EVM is stiffer than the MCSL EoS as one can see from the right panel of Fig. 9. Also from this figure one can see that the model is not valid at high temperatures: the conventional HRGM with multicomponent hard-core repulsion is valid for packing fractions $\eta \leq 0.11$, i.e. for $T < 200$ MeV. From the right panel of Fig. 9 one can find that this EoS provides a 5% deviation from the MCSL EoS at $T \simeq 215$ MeV. Therefore, we conclude that the HRGM EoS cannot be used at higher temperatures because it becomes too stiff even compared to the hard spheres and, hence, it leads to the superluminal speed of sound.

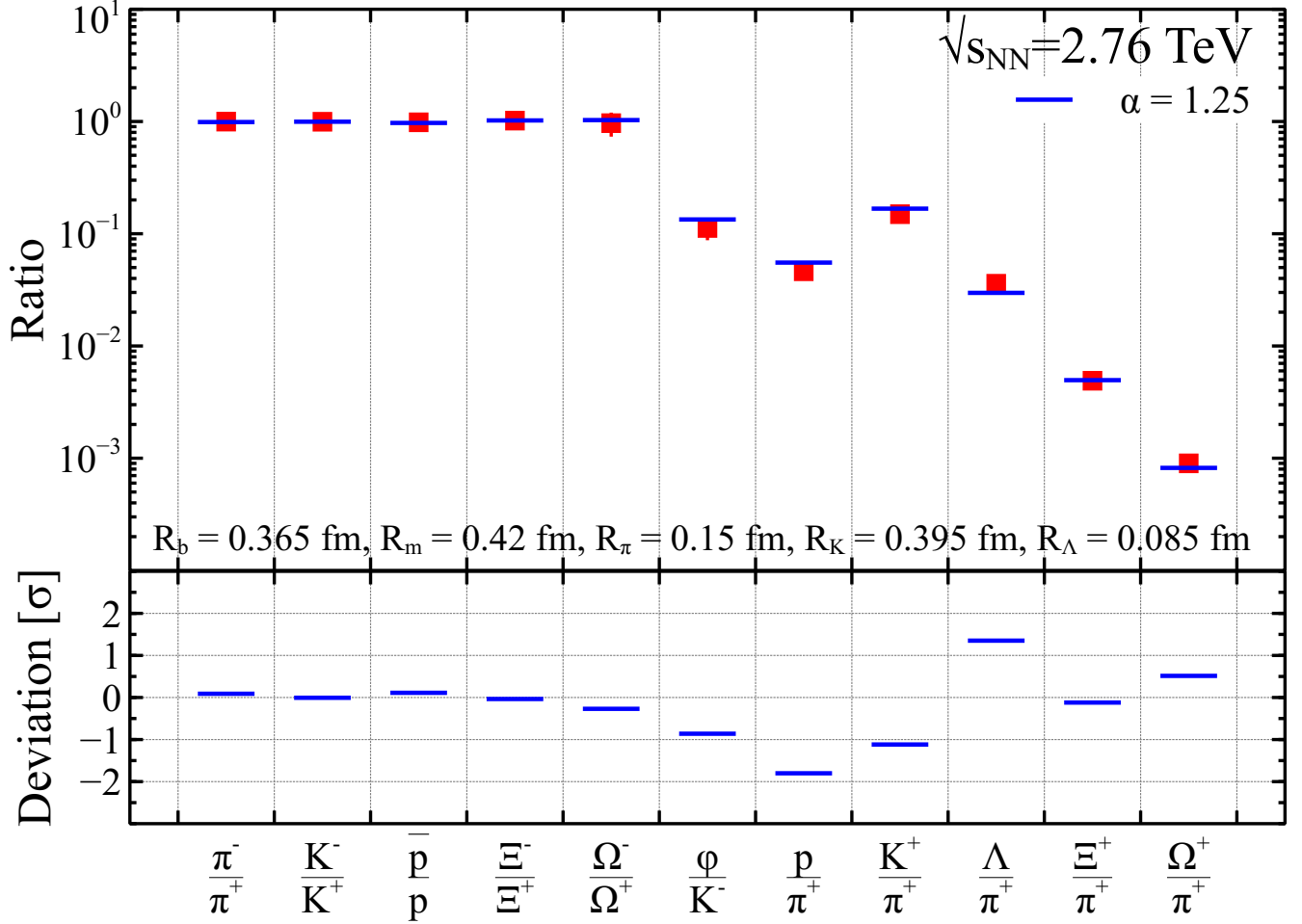


Figure 8: The ratios from Table 1 which were fitted by the IST EoS with the new radii found in this work. The obtained CFO temperature is $T_{CFO} \simeq 152 \pm 7 \text{ MeV}$. The quality of the fit is $\chi^2_2/dof \simeq 8.04/5 \simeq 1.61$. The upper panel shows the fit of the ratios, while the lower panel shows the deviation between data and theory in the units of error.

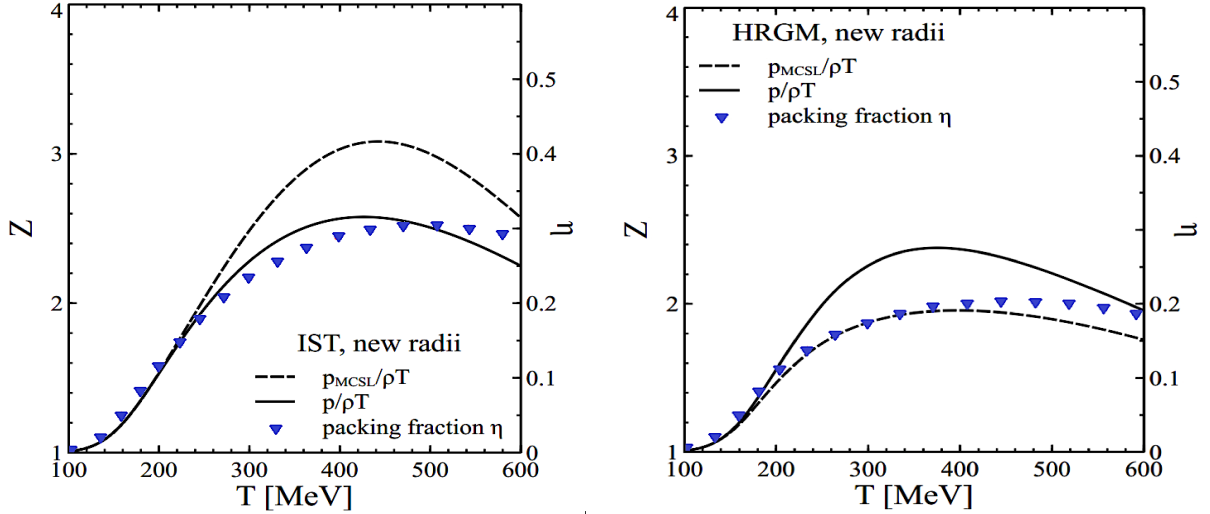


Figure 9: **Left panel:** Comparison of the thermal compressibility Z as the function of CFO temperature T is made for the IST EoS (solid curve) and for the MCSL EoS (dashed curve) found for the same particle densities for the hard-core radii of this work. **Right panel:** A similar comparison between the HRGM results obtained for the same set of hard-core radii (solid curve) and the MCSL EoS (dashed curve) is shown.

4 Conclusions

In this work we discussed an entirely new EoS of hadronic matter and the results obtained by this model. The developed EoS is a physically transparent generalization of the multicomponent Van der Waals EoS which correctly accounts for the third and fourth virial coefficients of the gas of hard spheres. This is shown by the direct evaluation of the third and fourth virial coefficients for the one-component case, i.e. when all particles have the same hard-core radius. A single value of the model parameter $\alpha = 1.25$ allows us to simultaneously reproduce the third and fourth virial coefficients of the gas of hard spheres with small deviations from their exact values. This very fact shows that the developed model catches the correct physics and we explicitly demonstrate that the parameter α plays the role of a “switcher” between the eigenvolume and excluded volume regimes. This conclusion is supported by a comparison of the compressibility factor Z and speed of sound of the IST EoS and the ones found by the Carnahan-Starling EoS [4] for the same particles and same hard-core radii.

Moreover, at vanishing baryonic densities we compared the compressibility factor Z of the IST EoS and the one calculated for the multicomponent version of the Carnahan-Starling EoS [56] known as the Mansoori-Carnahan-Starling-Leland EoS. This comparison shows that the conventional multicomponent HRGM corresponds to the MCSL EoS at the temperatures below 215 MeV, while the IST EoS reproduces the MCSL EoS compressibility factor Z with the relative error 5% up to the temperature 275 MeV. Furthermore, we found that in contrast to the conventional HRGM the IST EoS is essentially softer than the Carnahan-Starling and the MCSL EoS at high particle number densities. Thus, the developed EoS breaks causality at so high densities that in this region the hadronic description should be replaced by the quark gluonic one.

Using the IST EoS we described the AGS, SPS, RHIC and ALICE with rather high fit quality $\chi^2_{tot}/dof \simeq 1.08$. Compared to the hard-core radii found within the HRGM [17] only the pion hard-core radius changed from $R_\pi = 0.1$ fm to $R_\pi = 0.15$ fm and the hard-core radius of Λ (anti)hyperons decreased from $R_\Lambda = 0.11$ fm to $R_\Lambda = 0.085$ fm. The other hard-core radii are almost the same as

in Ref. [17]. These values of hard-core radii allow us to describe all the hadronic yield ratios well, including the energy dependence of the most problematic ones, i.e. K^+/π^+ , $\bar{\Lambda}/\pi^-$ and Λ/π^- ratios. Despite the change of hard-core radii of pions and Λ (anti)hyperons, the present analysis confirmed that the peak of strangeness enhancement exists at $\sqrt{s_{NN}} = 3.8$ GeV and that the sudden jump of the CFO temperature occurs between $\sqrt{s_{NN}} = 4.3$ GeV and $\sqrt{s_{NN}} = 4.9$ GeV. Furthermore, we argue that the appearance of chemical equilibrium of strangeness, i.e. $\gamma_s \simeq 1$ within the error bars, observed at $\sqrt{s_{NN}} = 4.9$ GeV maybe a new signal for the onset of deconfinement.

It is necessary to stress, that the great numerical advantage of the IST EoS over the existing EVM is that independently of the number of different hard-core radii one has to solve just two equations. Hence, we believe that such a property may open absolutely new possibilities in the future to extract the hard-core radii from the data with very high confidence, if the measurements at NICA and FAIR will provide much more precise data for hadron multiplicities.

Acknowledgments. The authors are thankful to A. Andronic, P. Braun-Munzinger, R. Emaus, M. Gazdzicki, D. R. Oliinychenko and D. H. Rischke for the fruitful discussions and for important comments. K.A.B., V.V.S., A.I.I and G.M.Z. acknowledge the partial support of the program “Nuclear matter under extreme conditions” launched by the Section of Nuclear Physics of National Academy of Sciences of Ukraine. K.A.B. acknowledges the partial support by the ExtreMe Matter Institute EMMI, GSI Helmholtzzentrum für Schwerionenforschung, Darmstadt, Germany. The work of D.B. and A.I.I. was supported in part by the Polish National Centre (NCN) under contract number UMO-2011/02/A/ST2/00306. D.B. is grateful for support by the MEPHI Academic Excellence Project under contract number 02.a03.21.0005. C.G. acknowledges a support from HIC for FAIR.

A Appendix

In order to heuristically derive the IST EoS, let us first remind the formal steps of obtaining the Van der Waals EoS in the grand canonical ensemble. For this purpose we consider first the one-component gas with the hard-core repulsion. The pressure of such a gas with the temperature T and chemical potential μ in the Boltzmann approximation is given by

$$p = T \phi(T) \exp \left[\frac{\mu - a p}{T} \right], \quad \text{with} \quad \phi(T) = g \int \frac{d^3 k}{(2\pi)^3} \exp \left[-\frac{\sqrt{k^2 + m^2}}{T} \right]. \quad (31)$$

Here $a = \frac{2}{3}\pi(2R)^3$ denotes an excluded volume per particle for the hard-core radius R and $\phi(T)$ is a thermal density of hadron having the mass m and the degeneracy factor g . In general case, which accounts for the finite width of hadronic resonances one has to use Eq. (4) for a thermal density. For low particle number densities Eq. (31) can be obtained from the virial expansion at low densities

$$p \simeq T \phi e^{\frac{\mu}{T}} \left(1 - a \phi e^{\frac{\mu}{T}} \right), \quad (32)$$

in the following sequence of steps [34]. First, in the second term staying in the brackets in Eq. (32) one has to approximate the particle density as $\phi e^{\frac{\mu}{T}} \simeq \frac{p}{T}$, using the fact that at low densities such an approximation is a correct one; second, the obtained term is further approximated as $1 - a \frac{p}{T} \simeq \exp \left[-a \frac{p}{T} \right]$. As a result Eq. (31) is reproduced. The final step is to extrapolate Eq. (31) to high densities.

Let us now apply the same steps to the system of N -sorts of hadrons with the hard-core radii R_k , with $k = 1, 2, \dots, N$. Then the virial expansion of the gas pressure up to second order in particle

density can be written as

$$p = T \sum_{k=1}^N \phi_k e^{\frac{\mu_k}{T}} \left(1 - \sum_{n=1}^N a_{kn} \phi_n e^{\frac{\mu_n}{T}} \right), \quad (33)$$

where $\phi_k(T)$ (4) is the thermal density of particles of the degeneracy g_k and mass m_k , μ_k denotes their chemical potential, while a_{kn} is the excluded volume of particles having the hard-core-radii R_k and R_n

$$a_{kn} = \frac{2}{3}\pi (R_k + R_n)^3 = \frac{2}{3}\pi (R_k^3 + 3R_k^2 R_n + 3R_k R_n^2 + R_n^3). \quad (34)$$

One can repeat the same steps as above with the only modification that for the multicomponent system each sort of particles, say k , generates its own pressure p_k which should replace in Eq. (33) the particle density as $\phi_n e^{\frac{\mu_n}{T}} \simeq \frac{p_n}{T}$. Then one obtains the system of equations for partial pressures

$$p_k = T \phi_k \exp \left[\frac{\mu_k}{T} - \sum_{n=1}^N a_{kn} \frac{p_n}{T} \right]. \quad (35)$$

Such an EoS is known as the Lorentz-Berthelot mixture for which the total pressure is the sum of all partial ones $p = \sum_{k=1}^N p_k$.

However, the procedure of the Van der Waals extrapolation is not unique and one can use a different approach. It is necessary to stress that an order of mathematical operations is important now [34]. If, in contrast to the steps above, one explicitly substitutes the excluded volume (4) into expression for pressure (33) first and regroups the powers of radius R_k of a hadron of sort k , then one can get a different expression

$$p = T \sum_{k=1}^N \phi_k e^{\frac{\mu_k}{T}} \left[1 - \frac{4}{3}\pi R_k^3 \cdot \sum_{n=1}^N \phi_n e^{\frac{\mu_n}{T}} - 2\pi R_k^2 \cdot \sum_{n=1}^N R_n \phi_n e^{\frac{\mu_n}{T}} - 2\pi R_k \cdot \sum_{n=1}^N R_n^2 \phi_n e^{\frac{\mu_n}{T}} \right]. \quad (36)$$

Noting that the third and the fourth terms on the right hand side of Eq. (36) are identical for low densities, we can write (36) as

$$p = T \sum_{k=1}^N \phi_k e^{\frac{\mu_k}{T}} \left[1 - \frac{4}{3}\pi R_k^3 \cdot \sum_{n=1}^N \phi_n e^{\frac{\mu_n}{T}} - 4\pi R_k^2 \cdot \sum_{n=1}^N R_n \phi_n e^{\frac{\mu_n}{T}} \right]. \quad (37)$$

Next we rewrite the terms staying in the square brackets in Eq. (37) via an exponential and obtain

$$p = T \sum_{k=1}^N \phi_k \exp \left[\frac{\mu_k}{T} - \frac{4}{3}\pi R_k^3 \cdot \frac{p}{T} - 4\pi R_k^2 \cdot \frac{\Sigma}{T} \right], \quad (38)$$

where we made the same approximation for total pressure as above $T \sum_{n=1}^N \phi_n e^{\frac{\mu_n}{T}} \simeq p$. A similar approximation has to be made for the induced surface tension coefficient Σ in order to guarantee a consistency with the derivation above and to have the correct values for all second virial coefficients at low densities. Hence we assume that the induced surface free energy coefficient Σ obeys the following equation

$$\Sigma = T \sum_{k=1}^N R_k \phi_k \exp \left[\frac{\mu_k}{T} - \frac{4}{3}\pi R_k^3 \cdot \frac{p}{T} - 4\pi R_k^2 \cdot \alpha \frac{\Sigma}{T} \right], \quad (39)$$

which is a complete analog of the equation (38) for pressure. The only difference with Eq. (38) is the presence of the constant $\alpha > 0$ which is introduced due to the freedom of the Van der Waals

extrapolation to high densities. By construction the finite values of α cannot affect the second virial coefficients, but with it help the present model is able to account for higher order corrections compared to the low density virial expansion.

From the derivation above it is clear that the induced surface tension coefficient $\Sigma > 0$ is generated by the hard-core repulsion and accounts for its essential part. As it is argued in [34] the attractive interaction will lead to $\Sigma < 0$.

References

- [1] N. K. Glendenning, “Compact Stars”, Springer-Verlag, New York (2000).
- [2] P. Haensel, A. Y. Potekhin and D. G. Yakovlev, *Astrophys. Space Sci. Libr.* **326** (2007).
- [3] N. F. Mott, *Metal - Insulator Transitions*, Taylor & Francis Ltd., New York (1974).
- [4] N. F. Carnahan and K. E. Starling, *J. Chem. Phys.* **51**, 635 (1969).
- [5] W. Ebeling, D. Blaschke, R. Redmer, H. Reinholz and G. Röpke, *J. Phys. A* **42**, 214033 (2009).
- [6] W. Ebeling, D. Blaschke, R. Redmer, H. Reinholz and G. Röpke, in: *Metal-to-Nonmetal Transitions*, Springer Series in Materials Science, vol. 132, Springer, Berlin (2010), p. 37.
- [7] J. M. Lattimer and F. D. Swesty, *Nucl. Phys. A* **535**, 331 (1991).
- [8] H. Shen, H. Toki, K. Oyamatsu and K. Sumiyoshi, *Nucl. Phys. A* **637**, 435 (1998).
- [9] S. Typel, G. Röpke, T. Klähn, D. Blaschke and H. H. Wolter, *Phys. Rev. C* **81**, 015803 (2010).
- [10] S. Benic, D. Blaschke, D. E. Alvarez-Castillo, T. Fischer and S. Typel, *Astron. Astrophys.* **577**, A40 (2015).
- [11] A. Andronic, P. Braun-Munzinger and J. Stachel, *Nucl. Phys. A* **772**, 167 (2006) and references therein.
- [12] J. Stachel, A. Andronic, P. Braun-Munzinger and K. Redlich, *J. Phys. Conf. Ser.* **509**, 012019 (2014) and references therein.
- [13] S. Typel, *Eur. Phys. J. A* **52**, 16 (2016).
- [14] K. A. Bugaev, D. R. Oliinychenko, A. S. Sorin and G. M. Zinovjev, *Eur. Phys. J. A* **49**, 30 (2013).
- [15] D. R. Oliinychenko, K. A. Bugaev and A. S. Sorin, *Ukr. J. Phys.* **58**, 211 (2013).
- [16] K. A. Bugaev et al., *Europhys. Lett.* **104**, 22002 (2013).
- [17] V. V. Sagun, *Ukr. J. Phys.* **59**, 755 (2014).
- [18] K. A. Bugaev et al., *Phys. Part. Nucl. Lett.* **12**, 351 (2015).
- [19] K. A. Bugaev et al., *Eur. Phys. J. A* **52**, 175 (2016).
- [20] K. A. Bugaev et al., arXiv:1611.07349v2 [nucl-th].

- [21] K. A. Bugaev et al., Ukr. J. Phys. **61**, 659 (2016).
- [22] K. A. Bugaev et al., Eur. Phys. J. A **52**, 227 (2016).
- [23] V. Vovchenko and H. Stöcker, arXiv:1512.08046v2 [hep-ph].
- [24] L. M. Satarov, K. A. Bugaev and I. N. Mishustin, Phys. Rev. C **91**, 055203 (2015).
- [25] K. A. Bugaev, Phys. Rev. C **76**, 014903 (2007).
- [26] K. A. Bugaev, V. K. Petrov and G. M. Zinovjev, Phys. Atom. Nucl. **76**, 341 (2013).
- [27] I. Zakout, C. Greiner, and J. Schaffner-Bielich, Nucl. Phys. A **781**, 150 (2007).
- [28] I. Zakout and C. Greiner, Phys. Rev. C **78**, 034916 (2008).
- [29] L. Ferroni and V. Koch, Phys. Rev. C **79**, 034905 (2009).
- [30] I. Zakout and C. Greiner, arXiv:1002.3119.
- [31] A. I. Ivanytskyi, Nucl. Phys. A **880**, 12 (2012).
- [32] A. I. Ivanytskyi, K. A. Bugaev, A. S. Sorin and G. M. Zinovjev, Phys. Rev. E **86**, 061107 (2012).
- [33] A. I. Ivanytskyi and K. A. Bugaev, Ukr. J. Phys. **57**, 964 (2012).
- [34] V. V. Sagun, K. A. Bugaev, A. I. Ivanytskyi, I.N. Mishustin, Nucl. Phys. A **924**, 24 (2014).
- [35] S. Das Gupta and A. Z. Mekjian, Phys. Rev. C **57**, 1361 (1998).
- [36] D. Blaschke, A. Dubinin and L. Turko, arXiv:1611.09845 [hep-ph].
- [37] D. Blaschke, A. Dubinin and L. Turko, arXiv:1612.09556 [hep-ph].
- [38] G. Baym, Phys. Rev. **127**, 1391 (1962).
- [39] B. Vanderheyden and G. Baym, J. Stat. Phys. **93**, 843 (1998).
- [40] J. Rafelski, Phys. Lett. B **62**, 333 (1991).
- [41] J. P. Hansen and I. R. McDonald, *“Theory of simple fluids”*, Academic Press, Amsterdam, 2006.
- [42] B. Abelev *et al.* [ALICE Collaboration], Phys. Rev. C **88**, 044910 (2013).
- [43] B. B. Abelev *et al.* [ALICE Collaboration], Phys. Lett. B **728**, 216 (2014); Erratum: [Phys. Lett. B **734**, 409 (2014)]
- [44] B. B. Abelev *et al.* [ALICE Collaboration], Phys. Rev. Lett. **111**, 222301 (2013).
- [45] A. G. Knospe [ALICE Collaboration], J. Phys. Conf. Ser. **509**, 012087 (2014).
- [46] J. Adam *et al.* [ALICE Collaboration], Phys. Rev. C **93**, 024917 (2016).
- [47] B. Dönigus [ALICE Collaboration], EPJ Web Conf. **97**, 00013 (2015).

- [48] J. Adam *et al.* [ALICE Collaboration], Phys. Lett. B **754**, 360 (2016).
- [49] S. Wheaton, J. Cleymans and M. Hauer, Comput. Phys. Commun. **180**, 84 (2009).
- [50] R. Hagedorn, Nuovo Cim. Suppl. **3**, 147 (1965).
- [51] L. G. Moretto, K. A. Bugaev, J. B. Elliott and L. Phair, Europhys. Lett. **76**, 402 (2006).
- [52] M. Beitel, K. Gallmeister and C. Greiner, Phys. Rev. C **90**, 045203 (2014).
- [53] M. Beitel, K. Gallmeister and C. Greiner, J. Phys. Conf. Ser. **668**, 012057 (2016).
- [54] M. Beitel, C. Greiner and H. Stoecker, Phys. Rev. C **94**, 021902 (2016).
- [55] S. Chatterjee *et al.*, Adv. High Energy Phys. **2015**, 349013 (2015).
- [56] G. A. Mansoori, N. F. Carnahan, K. E. Starling and T. W. Leland, Jr., J. Chem. Phys. **54**, 1523 (1971).
- [57] J. P. Hansen and I. R. McDonald, *“Theory of simple liquids”*, Academic, London (2006).
- [58] J. J. Salacuse and G. Stell, J. Chem. Phys. **77**, 3714 (1982).